Thermodynamics of Nucleotide Binding to Actomyosin V and VI: A Positive Heat Capacity Change Accompanies Strong ADP Binding†

James P. Robblee, Wenxiang Cao, Arnon Henn, Diane E. Hannemann, and Enrique M. De La Cruz*

Yale University, Department of Molecular Biophysics and Biochemistry, 260 Whitney Avenue, New Haven, Connecticut 06520

Received February 8, 2005; Revised Manuscript Received May 20, 2005

ABSTRACT: We have measured the energetics of ATP and ADP binding to single-headed actomyosin V and VI from the temperature dependence of the rate and equilibrium binding constants. Nucleotide binding to actomyosin V and VI can be modeled as two-step binding mechanisms involving the formation of collision complexes followed by isomerization to states with high nucleotide affinity. Formation of the actomyosin VI−ATP collision complex is much weaker and slower than for actomyosin V. A three-step binding mechanism where actomyosin VI isomerizes between two conformations, one competent to bind ATP and one not, followed by rapid ATP binding best accounts for the data. ADP binds to actomyosin V more tightly than actomyosin VI. At 25 °C, the strong ADP-binding equilibria are comparable for actomyosin V and VI, and the different overall ADP affinities arise from differences in the ADP collision complex affinity. The actomyosin−ADP isomerization leading to strong ADP binding is entropy driven at >15 °C and occurs with a large, positive change in heat capacity ($\Delta C_P°$) for both actomyosin V and VI. Sucrose slows ADP binding and dissociation from actomyosin V and VI but not the overall equilibrium constants for strong ADP binding, indicating that solvent viscosity dampens ADP-dependent kinetic transitions, presumably a tail swing that occurs with ADP binding and release. We favor a mechanism where strong ADP binding increases the dynamics and flexibility of the actomyosin complex. The heat capacity ($\Delta C_P°$) and entropy ($\Delta S°$) changes are greater for actomyosin VI than actomyosin V, suggesting different extents of ADP-induced structural rearrangement.

Myosins are molecular motors that utilize the energy from adenosine 5′-triphosphate (ATP)[1] binding, hydrolysis, and product release to perform mechanical work along actin filament tracks for diverse physiological processes including muscle contraction, cell division, vesicle and RNA transport, and chemotaxis (*1*, *2*). Force generation and motility (work output) are coupled to chemical catalysis. ATP binding and hydrolysis cycle myosin vectorially through a series of energetic (conformational) states that bind actin filaments strongly (attached) or weakly (detached) depending on the chemical state of the bound nucleotide. In the absence of nucleotide or with bound adenosine 5′-diphosphate (ADP), myosin binds actin filaments strongly (strong binding states). With ATP and the hydrolysis products, ADP and phosphate (P_i), bound myosin binds actin weakly (weak binding states). The fraction of the catalytic cycle time spent strongly attached to actin is referred to as the duty ratio.

Although all characterized myosins share a common ATPase cycle pathway, detailed kinetic analyses indicate that modulation of the rate and equilibrium constants that define the ATPase cycle confer specific properties to the motor for specific physiological tasks (*3*). Some myosins are tuned for anchoring cellular structures and maintaining tension, while others are better suited for transporting cargo or generating rapid sliding velocities. Muscle myosin is not processive. It tugs intermittently on actin filaments but is dissociated much of the time; therefore, multiple myosins are needed to sustain constant movement. Myosin V is processive, and an individual, two-headed motor molecule takes multiple steps and walks along an actin filament for long distances without detaching. Recent evidence suggests that myosin VI is a monomer (*4*), but an engineered myosin VI dimer is processive (*5*−*7*), albeit less than myosin V (*8*). Myosin V and VI undergoing processive motility coordinate their catalytic ATPase cycles (*5*, *9*−*12*).

Each head of a processive double-headed myosin, where single heads are not independently processive, must have a have a high duty ratio so that at least one motor is attached to actin at all times or else random thermal forces would cause it to diffuse away from its track. High duty ratios are achieved by favoring rapid and essentially irreversible entry into the strong binding states and a slow flux from strongly bound to weakly bound states (*13*, *14*). The equilibrium constant for ATP hydrolysis must favor the hydrolysis products (*14*). Rapid actin-activated P_i release and slow, rate-limiting ADP release largely account for the high duty ratios of myosins V and VI in the presence of actin (*5*, *13*−*15*), but slow and weak ATP binding also contribute to the high duty ratio of myosin VI (*5*, *10*).

While the kinetic basis of the myosin V and VI duty ratios are well-established (*5*, *13*, *14*), essentially no information

† This work was supported by grants from the National Science Foundation (MCB-0216834) and the American Heart Association (Scientist Development Grant 0235203N) to E.M.D.L.C. W.C. is supported by an Anderson endowed postdoctoral fellowship from Yale University. A.H. is supported by an American Heart Association postdoctoral fellowship.

* To whom correspondence should be addressed. Telephone: (203) 432-5424. Fax: (203) 432-1296. E-mail: enrique.delacruz@yale.edu.

[1] Abbreviations: ADP, adenosine 5′-diphosphate; ATP, adenosine 5′-triphosphate.

10.1021/bi050232g CCC: $30.25
Published on Web 07/09/2005

regarding the thermodynamic basis of the high ADP affinities that help dictate the duty ratios is available. In this study, we have investigated the energetics of nucleotide binding to myosins V and VI from the physical linkage of the rate and equilibrium constants to temperature. Our results indicate that strong ADP binding to myosins V and VI occurs with a positive heat capacity change, consistent with significant nucleotide-dependent conformational rearrangement and population of multiple conformational states contributing to the stability of the actomyosin−ADP complex. In addition, the kinetic data favor a mechanism where a conformational change precedes ATP binding to actomyosin VI.

EXPERIMENTAL PROCEDURES

Reagents. All chemicals were the highest purity commercially available. ATP (99+% purity as assayed by HPLC, data not shown) was purchased from Roche Molecular Biochemicals (Indianapolis, IN), and ADP (Sigma A-5285, 99+% purity as assayed by HPLC, data not shown) was purchased from Sigma (St. Louis, MO). ATP and ADP concentrations were determined by absorbance at 259 nm using a ϵ_{259} of 15 400 M^{-1} cm^{-1}. A molar equivalent of $MgCl_2$ was added to nucleotides immediately before use. Pyrenyl-iodoacetamide came from Molecular Probes (Eugene, OR). Fluorescence-grade (99+%, titration) imidazole and phalloidin were purchased from Sigma. Ultrapure sucrose was from American Bioanalytical.

Protein Expression and Purification. Single-headed chicken myosin V-1IQ with bound LC-1sa light chain (*13*, *14*) and single-headed porcine myosin VI (T406A mutant) with bound calmodulin light chain (*5*, *10*) were purified from Sf9 cells by Flag affinity chromatography (*16*). Purity was >98% for all preparations, with actin being the only detectible contaminant.

Actin was purified from rabbit skeletal muscle (*17*), labeled with pyrene (*18*), and gel-filtered over Sephacryl S-300HR. Ca^{2+}-actin monomers were converted to Mg^{2+}-actin monomers with 0.2 mM EGTA and 50 μM $MgCl_2$ (excess over [actin]) immediately prior to polymerization by dialysis into KMg50 buffer (3 × 500 mL). Phalloidin (1.1 M equiv) was used to stabilize actin filaments.

Stopped-Flow Measurements and Kinetic Modeling. All experiments were performed in KMg50 buffer (50 mM KCl, 2 mM $MgCl_2$, 1 mM EGTA, 1 mM DTT, and 10 mM imidazole at pH 7.0) with an Applied Photophysics (Surrey, U.K.) SX.18MV-R stopped-flow apparatus thermostated at the indicated temperatures (±0.1 °C). The buffer pH was adjusted at the experimental temperatures. Pyrene (λ_{ex} = 366 nm) fluorescence were monitored through a 400 nm long pass colored glass filter. Long time courses of pyrene fluorescence change were corrected for photobleaching by subtracting the time courses of fluorescence acquired after mixing pyrene actin filaments with nucleotides. Essentially identical results were obtained when the time courses after mixing actomyosin and buffer were subtracted.

Most of the time courses shown are of individual, unaveraged, 1000-point transients collected with the instrument in oversampling mode. The intrinsic time constant for data acquisition is ~30 μs. Time courses that display fast and slow phases were collected on a logarithmic time scale. Typically, multiple (3−8) time courses were averaged before analysis. Nonlinear least-squares fitting was done using Pro-K software provided with the instrument or with Kaleidagraph (Synergy Software, Reading, PA). Uncertainties are reported as standard errors in the fits unless stated otherwise. Concentrations stated are final after mixing.

Time courses of fluorescence enhancement were fitted to a sum of exponentials (eq 1)

$$F(t) = F_\infty + \sum_{i=1}^{n} A_i e^{-k_i t} \quad (1)$$

where $F(t)$ is the fluorescence at time t, F_∞ is the fluorescence intensity at infinity, A_i is the amplitude, k_i is the observed rate constant characterizing the ith relaxation process, and n is the total number of observed relaxations. The value of n was 1 (single exponential), 2 (double exponential), or 3 (triple exponential).

Time courses of fluorescence enhancement displaying a lag phase were fitted to a double-exponential function with comparable rate constants (*19*, *20*), where the faster exponential term has a positive amplitude (A_i) that generates the observed lag phase (*19*).

Kinetic simulations of reaction time courses were performed with KinTekSim (provided by Dr. Ken Johnson, University of Texas, Austin, TX, available free from KinTek Corporation at http://www.kintek-corp.com) and Tenua (provided by Dr. Daniel Wachsstock, available free at http://www.geocities.com/tenua4java/). Both programs are based on the kinetic simulation program KINSIM developed by Carl Frieden and colleagues [(*21*), available free at http://biochem.wustl.edu/cflab/].

Nucleotide-Binding Kinetics. Time courses of nucleotide binding were acquired under pseudo-first-order conditions with [nucleotide] ≫ [actomyosin]. Actomyosin samples were prepared by mixing myosin with 1.1 M equiv of pyrene actin filaments and equilibrating at 25 °C for at least 5 min. Apyrase (potato-grade VII, 0.1 unit mL^{-1} final) was added to ensure rigor (no nucleotide) conditions when indicated.

ATP binding was measured from the fluorescence of pyrene actin filaments (*5*, *10*, *13*). ADP binding to pyrene actomyosin was measured by kinetic competition with ATP (*10*).

Temperature Dependence of the Equilibrium Constants. The free-energy changes of the individual nucleotide-binding reactions were calculated using the Gibbs free-energy equation (eq 2), which relates the standard free-energy change ($\Delta G°$) to the association equilibrium constant (K) according to

$$\Delta G° = -RT \ln K \quad (2)$$

where R is the gas constant (1.98 cal mol^{-1} K^{-1}) and T is the absolute temperature in Kelvin. Expanding the standard free-energy change into its enthalpic ($\Delta H°$) and entropic ($\Delta S°$) components and rearranging yields

$$\ln K = -\frac{\Delta H°}{RT} + \frac{\Delta S°}{R} \quad (3)$$

permitting determination of the standard enthalpy change ($\Delta H°$) from the slope of the line generated by ln K versus $1/T$ (i.e., van't Hoff plot). The intercept is not an accurate estimate of the standard entropy change ($\Delta S°$) because it is

beyond the range of the data; therefore, it was calculated at a specific temperature from

$$\Delta S^\circ = \frac{\Delta H^\circ - \Delta G^\circ}{T} \quad (4)$$

Nonlinear van't Hoff plots were fitted to an integrated form of eq 3 (*22*) to account for the temperature dependence of ΔH° that arises from a change in the standard molar heat capacity (ΔC_P°), which was assumed to be constant and independent of the temperature over the range examined

$$\ln K = \frac{\Delta S^\circ_{T_R}}{R} - \frac{\Delta H^\circ_{T_R}}{RT} + \frac{\Delta C^\circ_P}{R}\left(\ln\left(\frac{T}{T_R}\right) + \frac{T_R}{T} - 1\right) \quad (5)$$

where subscript R refers to values at a selected reference temperature.

Solvent Manipulations. Solvent viscosities (η) and osmotic pressures (π) were adjusted with sucrose. The viscosities and osmotic pressures of the solutions were obtained from ref *23* and the Brock University osmotic stress website (http://aqueous.labs.brocku.ca/osfile.html), respectively.

The dependence of the association equilibrium constants for nucleotide binding on water activity was interpreted by considering water as a ligand (*24*). The number of water molecules involved in the formation of the ATP collision complex (K_{1T}), ADP collision complex (K_{1D}), and ADP isomerization equilibrium (K_{2D}) were determined according to the following relationship

$$\ln K = \frac{-\Delta n[\text{osmolal}]}{55.6} \quad (6)$$

where Δn is the change in the number of bound water molecules obtained from the best fit line describing the relationship between the natural log of the association equilibrium constants and osmolal solute (sucrose) concentration.

Error Propagation. Uncertainties were propagated using the formula (eq 7)

$$da = \sqrt{\left(\frac{\partial a}{\partial x_1}dx_1\right)^2 + ... + \left(\frac{\partial a}{\partial x_n}dx_n\right)^2} \quad (7)$$

where the experimental measurements x_1, x_2, ..., x_n have uncertainties dx_1, dx_2, ..., dx_n and a is a function of x_1, x_2, ..., x_n.

RESULTS

A. Mechanism and Temperature Dependence of ATP Binding to Actomyosin V. ATP binding to pyrene actomyosin V was monitored from the fluorescence enhancement of pyrene actin that arises from the population of the actin weak binding states (*13*, *15*). Time courses of fluorescence enhancement after mixing ATP with pyrene actomyosin V follow single exponentials with observed rate constants that depend hyperbolically on the ATP concentration (*13*, *15*) at all temperatures (4−25 °C) examined (Figure 1B). At higher temperatures, the maximum rates were too rapid to measure reliably (data not shown). The mechanism of ATP binding was modeled as a two-step process with formation of a low fluorescence collision complex [AM(ATP)] followed by isomerization (k_{+2T}) to a weak actin-binding state with high fluorescence (A*M·ATP) that rapidly dissociates ($k_{diss} \gg k_{+2T} + k_{-2T}$) from actin (Scheme 1; A* denotes a high (unquenched) pyrene fluorescence).

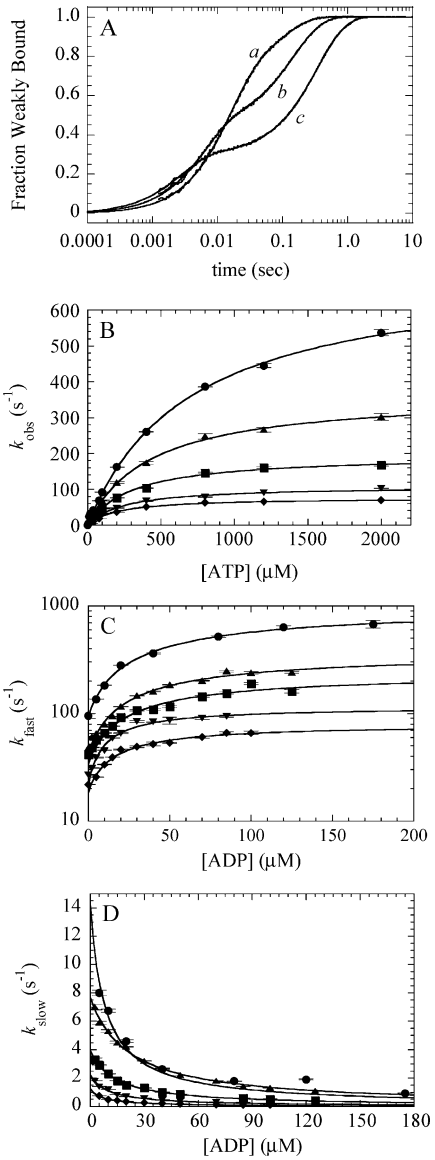

FIGURE 1: Temperature dependence of ADP binding to actomyosin V measured by kinetic competition. (A) Time courses (25 °C) of pyrene fluorescence enhancement after mixing 0.25 μM pyrene actomyosin V−S1 with 100 μM ATP supplemented with 2 μM ADP (curve a), 10 μM ADP (curve b), or 40 μM ADP (curve c). Concentrations are final after mixing. Smooth lines through the data represent fits to a double exponential. (B) [ATP] dependence of the observed rate (k_{obs}) of ATP binding to pyrene actomyosin V at 25 (●), 19 (▲), 14 (■), 9 (▼), and 4 (◆) °C. The solid lines are the best fits to a rectangular hyperbola (eq 12). The maximum rates of ATP binding (k_{+2T}) and the collision complex affinity ($1/K_{1T}$) used in the fits are those reported in Table 1. (C) [ADP] dependence of the fast relaxation rate constant at 25 (●), 19 (▲), 14 (■), 9 (▼), and 4 (◆) °C in the presence of 100 μM ATP (25 °C) or 70 μM ATP (19−4 °C). The solid lines are the best fits to eq 14. The maximum rates of ADP binding (k_{+2D}) and the collision complex affinity ($1/K_{1D}$) used in the fits are reported in Table 1. The ordinate was plotted on a logarithmic scale for clarity. (D) [ADP] dependence of the slow phase observed rate constant at 25 (●), 19 (▲), 14 (■), 9 (▼), and 4 (◆) °C in the presence of 100 μM ATP (25 °C) or 70 μM ATP (19−4 °C). The solid lines are the best fits to eq 15 with intercepts reported in Table 1 as k_{-2D} (ADP release).

Scheme 1

$$\mathrm{AM + ATP} \underset{k_{-1T}}{\overset{k_{+1T}}{\rightleftarrows}} \mathrm{AM(ATP)} \underset{k_{-2T}}{\overset{k_{+2T}}{\rightleftarrows}} \mathrm{A^*M.ATP} \xrightarrow{k_{diss}} \mathrm{A^* + M.ATP}$$

Solving the differential equations that govern Scheme 1 yields two observed rate constants (λ_1 and λ_2) defined by (*25*)

$$\lambda_{1,2} = \frac{b \pm \sqrt{b^2 - 4c}}{2} \tag{8}$$

where

$$b = k_{+1T}[\mathrm{ATP}] + k_{-1T} + k_{+2T} + k_{-2T}$$

$$c = k_{-2T}k_{+1T}[\mathrm{ATP}] + k_{-2T}k_{-1T} + k_{+2T}k_{+1T}[\mathrm{ATP}] \tag{9}$$

Under conditions where $k_{+1T}[\mathrm{ATP}] \gg k_{+2T} + k_{+2T}$, the two observed rate constants ($\lambda_1 > \lambda_2$, fast phase λ_1 and slow phase λ_2) simplify to

$$\lambda_1 = k_{+1T}[\mathrm{ATP}] + k_{-1T} \tag{10}$$

and

$$\lambda_2 = k_{-2T} + k_{+2T}\left(\frac{k_{+1T}[\mathrm{ATP}]}{k_{+1T}[\mathrm{ATP}] + k_{-1T}}\right) \tag{11}$$

Under our experimental conditions, $k_{-2T} \sim 0$ (i.e., $k_{diss} > k_{+2T} + k_{-2T}$); therefore, eq 11 simplifies further to

$$\lambda_2 = \frac{k_{+1T}k_{+2T}[\mathrm{ATP}]}{k_{-1T} + k_{+1T}[\mathrm{ATP}]} = \frac{K_{1T}k_{+2T}[\mathrm{ATP}]}{1 + K_{1T}[\mathrm{ATP}]} \tag{12}$$

where $K_{1T} = k_{+1T}/k_{-1T}$ is the association equilibrium constant of the collision complex.

The observed time courses of fluorescence enhancement are given by

$$\frac{[\mathrm{A^*M{\cdot}ATP}] + [\mathrm{A^* + M{\cdot}ATP}]}{[\mathrm{AM}]_o} = \left(\frac{k_{+2T}k_{+1T}[\mathrm{ATP}]\lambda_2}{(\lambda_1 - \lambda_2)c}\right)e^{-\lambda_1 t} - \left(\frac{k_{+2T}k_{+1T}[\mathrm{ATP}]\lambda_1}{(\lambda_1 - \lambda_2)c}\right)e^{-\lambda_2 t} + \left(\frac{k_{+1T}[\mathrm{ATP}]}{c}\right)k_{+2T} \tag{13}$$

where $[\mathrm{AM}]_o$ is the initial strongly bound and quenched pyrene actomyosin concentration and c is defined by eq 9. The first term on the right-hand side of eq 13 is an exponential decay. The second term describes an exponential fluorescence signal rise because of its negative amplitude (A_i in eq 1). When λ_1 in Scheme 2 is too fast to be resolved given the ~1−2 ms dead time of the instrument (i.e., >1000 s^{-1}), k_{+1T} and k_{-1T} cannot be measured directly and time courses will follow a single-exponential rise with the rate constant λ_2. The experimentally observed λ_2 rate constant will display a hyperbolic [ATP] dependence, allowing the equilibrium constant for collision complex formation ($K_{1T} = k_{+1T}/k_{-1T}$) and the isomerization rate constant (k_{+2T}) to be determined using eq 12.

Scheme 2

$$\begin{array}{ccccccc} \mathrm{AM + ATP} & \underset{k_{-1T}}{\overset{k_{+1T}}{\rightleftarrows}} & \mathrm{AM(ATP)} & \underset{k_{-2T}}{\overset{k_{+2T}}{\rightleftarrows}} & \mathrm{A^*M.ATP} & \xrightarrow{k_{diss}} & \mathrm{A^* + M.ATP} \\ + & & & & & & \\ \mathrm{ADP} & & & & & & \\ k_{-1D} \uparrow\downarrow k_{+1D} & & & & & & \\ \mathrm{AM(ADP)} & & & & & & \\ k_{-2D} \uparrow\downarrow k_{+2D} & & & & & & \\ \mathrm{AM.ADP} & & & & & & \end{array}$$

The equilibrium constant for formation of the actomyosin V collision complex [$1/K_{1T} = k_{-1T}/k_{+1T} = 697$ (±38) μM], the maximum observed rate constant [$k_{+2T} = 717$ (±17) s^{-1}], and the second-order association rate constant [$K_{1T}k_{+2T} = 1.03$ (±0.06) μM^{-1} s^{-1}] obtained at 25 °C in this study are comparable to published values ($1/K_{1T} = 967$ μM, $k_{+2T} = 870$ s^{-1}, and $K_{1T}k_{+2T} = 0.9$ μM^{-1} s^{-1}) acquired under comparable conditions (*13*).

B. Mechanism of ADP Binding to Actomyosin V at 25 °C. ADP binding to pyrene actomyosin V was measured by kinetic competition with ATP (*10*) as described by the following parallel binding reaction mechanisms (Scheme 2, A* denotes unquenched pyrene fluorescence).

When a solution of ADP and ATP is rapidly mixed with pyrene actomyosin V, time courses are biphasic and can be well-fitted to double exponentials (Figure 1A) with fast (Figure 1C) and slow (Figure 1D) phases that depend hyperbolically on [ADP] when the [ATP] is constant. The hyperbolic [ADP] dependence of the fast phase indicates that ADP binding to actomyosin V is a two-step process [(*10*); Scheme 2) where both the AM(ADP) and AM·ADP states bind actin strongly and remain attached to actin filaments at the protein concentrations used, but only the AM·ADP state binds nucleotide strongly.

The observed rate constant of the fast phase (k_{fast}) reflects depletion of free actomyosin and depends on the sum of the observed rate constants for ATP and ADP binding, which can be expressed in terms of the rate and equilibrium constants for nucleotide binding when nucleotide binding is irreversible [k_{-2T} and $k_{-2D} \sim 0$, essentially fulfilled in this case because dissociation is much slower than binding, see below (*10*)]

$$k_{fast} = \left(\frac{K_{1T}k_{+2T}[\mathrm{ATP}] + K_{1D}k_{+2D}[\mathrm{ADP}]}{1 + K_{1T}[\mathrm{ATP}] + K_{1D}[\mathrm{ADP}]}\right) \tag{14}$$

where $K_{1T} = k_{+1T}/k_{-1T}$ and $K_{1D} = k_{+1D}/k_{-1D}$ are the association equilibrium binding constant for the formation of ATP and ADP collision complexes, respectively. Fitting the [ADP] dependence of k_{fast} to eq 14 with K_{1T} and k_{+2T} constrained to the values obtained independently from ATP-binding experiments (Figure 1B and Table 1) yields a k_{+2D} of 973 (±45) s^{-1} and $1/K_{1D}$ of 74 (±8) μM at 25 °C for ADP binding to actomyosin V (Figure 1C and Table 1). The second-order association rate constant for ADP binding at 25 °C ($K_{1D}k_{+2D}$) is 13.1 (±1.4) μM^{-1} s^{-1}, within a factor of 2 of the value obtained with mantADP (*13*, *25*), indicating that fluorescent modification of the nucleotide has minimal effects on binding to actomyosin V.

The observed slow phase of the reaction arises from AM·ADP formed during kinetic partitioning in the fast phase that

Table 1: Rate and Equilibrium Constants for Nucleotide Binding to Actomyosin V and VI[a]

	25 °C	19 °C	14 °C	9 °C	4 °C
			actomyosin V		
ATP binding					
$1/K_{1T}$ (μM)	697 (±38)	426 (±24)	306 (±40)	266 (±32)	202 (±25)
k_{+2T} (s^{-1})	717 (±17)	367 (±7)	196 (±8)	111 (±4)	76.6 (±2.8)
ADP binding					
$K_{2D} = k_{+2D}/k_{-2D}$	68.5 (±4.6)	49.6 (±3.5)	51.0 (±4.2)	52.6 (±5.5)	66.6 (±3.2)
k_{+2D} (s^{-1})	973 (±45)	382 (±22)	199 (±13)	115.7 (±6.0)	79.9 (±3.6)
k_{-2D} (s^{-1})[b]	14.2 (±0.7)	7.7 (±0.3)	3.9 (±0.2)	2.2 (±0.2)	1.20 (±0.02)
k_{-2D} (s^{-1})[c]	13.0 (±0.1)	7.5 (±0.1)	4.2 (±0.1)	2.2 (±0.1)	1.02 (±0.01)
$1/K_{1D}$ (μM)	74.1 (±8.2)	62.3 (±9.3)	39.5 (±4.5)	17.9 (±3.0)	23.4 (±3.5)
			actomyosin VI		
ATP binding					
$1/K_{1T}$ (mM)	5.6 (±0.7)	7.2 (±0.8)	8.4 (±0.9)	9.0 (±0.5)	9.2 (±0.6)
k_{+2T} (s^{-1})	176.5 (±8.2)	165.2 (±7.7)	124.8 (±5.9)	93.4 (±2.5)	66.0 (±2.0)
ADP binding					
$K_{2D} = k_{+2D}/k_{-2D}$	64.2 (±6.6)	38.1 (±1.6)	38.6 (±3.2)	44.4 (±4.0)	62.0 (±6.6)
k_{+2D} (s^{-1})	366 (±32)	221.0 (±8.4)	150.5 (±12.0)	102.1 (±8.0)	91.2 (±9.0)
k_{-2D} (s^{-1})[b]	5.7 (±0.3)	5.8 (±0.1)	3.9 (±0.1)	2.3 (±0.1)	1.47 (±0.06)
k_{-2D} (s^{-1})[c]	6.9 (±0.1)	5.2 (±0.1)	3.5 (±0.1)	2.2 (±0.1)	1.15 (±0.02)
$1/K_{1D}$ (mM)	2.2 (±0.5)	1.1 (±0.2)	1.3 (±0.3)	1.2 (±0.3)	0.64 (±0.17)

[a] Conditions: 50 mM KCl, 2 mM $MgCl_2$, 1 mM EGTA, 1 mM DTT, and 10 mM imidazole at pH 7.0. [b] Obtained from the *y* intercept of the fit to the slow phase of the kinetic competition assay. [c] Measured from competing off a pre-equilibrated mixture of pyrene actomyosin−ADP with ATP.

dissociates bound ADP then binds ATP to populate the high fluorescence, weak actin-binding states (*10*). The ADP release rate constant (k_{-2D}) can be readily obtained from the best fit of the ADP concentration dependence of the slow phase (k_{slow} versus [ADP], Figure 1D) to eq 15 and extrapolating to the limit of [ADP] = 0 [i.e., the intercept, where $k_{ADP} = 0$ thus $k_{slow} = k_{-2D}$ (*10*)]

$$k_{slow} = \frac{k_{-2D}k_{ATP}}{(k_{ATP} + k_{ADP})} \quad (15)$$

where k_{ATP} and k_{ADP} represent the observed rate constants for ATP and ADP binding according to

$$k_{ATP} = \left(\frac{K_{1T}k_{+2T}[ATP]}{1 + K_{1T}[ATP] + K_{1D}[ADP]}\right) \quad (16)$$

and

$$k_{ADP} = \left(\frac{K_{1D}k_{+2D}[ADP]}{1 + K_{1T}[ATP] + K_{1D}[ADP]}\right) \quad (17)$$

The rate constant for ADP release from actomyosin V (k_{-2D}) at 25 °C obtained from the intercept of the best fit of the data is 14.2 (±0.7) s^{-1} (Figure 1D and Table 1), in reasonable agreement with the previously determined values of ∼12−18 s^{-1} (*13*, *25*−*27*). The equilibrium constant for strong ADP binding calculated from the ratio of the rate constants ($K_{2D} = k_{+2D}/k_{-2D}$) is ∼70 (Table 1). The overall dissociation equilibrium constant for ADP binding $(K_{1D}K_{2D})^{-1}$ to actomyosin V at 25 °C, calculated from the ratio of the rate constants ($k_{-2D}/K_{1D}k_{+2D}$), is 1.1 (±0.1) μM, comparable to the published values (*13*, *14*, *25*, *26*, *28*).

Recent studies show that time courses of mantADP binding to actomyosin V follow double exponentials (*29*) with [mantADP]-dependent fast observed rate constants and slow observed rate constants of ∼1 s^{-1} (*25*) that are independent of the nucleotide concentration, indicating that an additional slow isomerization follows strong ADP binding. We could not detect the slow isomerization observed with mantADP using the pyrene actin kinetic competition assay (i.e., time courses of pyrene fluorescence change follow only double exponentials with [ADP]-dependent rate constants at all nucleotide concentrations examined). The slow isomerization would not be resolved at low [ADP] because actomyosin−ADP populated during the initial kinetic partitioning releases bound ADP, binds ATP, and relaxes back to the weak actin-binding states more rapidly than the slow isomerization occurs. Simulations (not shown) indicate that the slow isomerization contributes to the time course of pyrene fluorescence enhancement at >50 μM ADP. However, at high [ADP], the contributions from the isomerization are small and difficult to distinguish in the time courses because the observed rate constant of the isomerization is comparable to the observed slow phase in the kinetic competition assay.

C. Temperature Dependence of ADP Binding to Actomyosin V. ADP binding follows a two-step mechanism over the temperature range examined (4−25 °C) as indicated from the hyperbolic concentration dependence of the observed fast rate constant (k_{fast}, Figure 1C). Because the kinetic competition assay requires knowledge of the ATP-binding constants, which we could not determine reliably, two-step ADP binding could not be measured at temperatures above 25 °C. The temperature dependence of the rate and equilibrium constants of ADP binding to actomyosin V are summarized in Table 1. The energetics will be discussed together with actomyosin VI below.

D. Mechanism and Temperature Dependence of ATP Binding to Actomyosin VI. Time courses of ATP binding to pyrene actomyosin VI follow single exponentials at temperatures ≥9 °C (curves a−d of Figure 2A) with observed rate constants that depend hyperbolically on the [ATP] (Figure 2C). At 4 °C (curve e of Figure 2A), time courses of fluorescence enhancement do not follow single exponentials but display an additional lag phase. The lag is absent in the time courses of ATP binding to actomyosin V at 4 °C (Figure

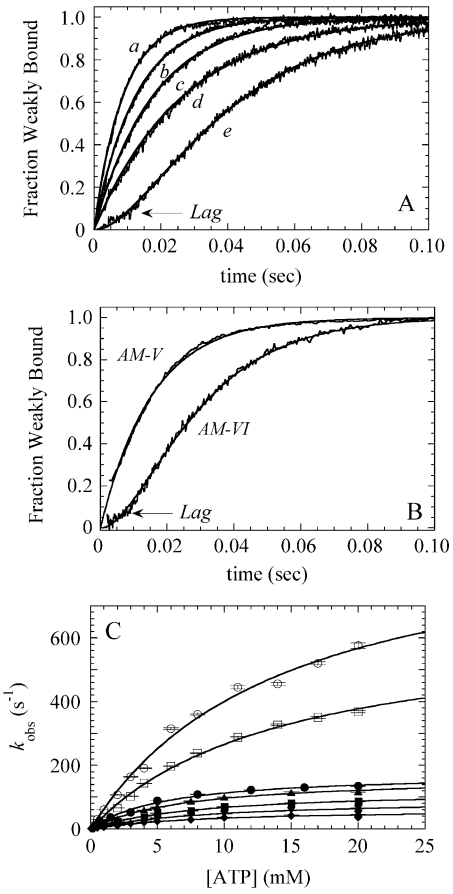

FIGURE 2: Time courses of ATP binding to actomyosin VI at different temperatures. (A) Time courses of fluorescence change after mixing 20 mM ATP with 0.5 μM actomyosin VI at 25 (curve a), 19 (curve b), 14 (curve c), 9 (curve d), and 4 (curve e) °C. Concentrations are final after mixing. Data are of individual, unaveraged transients. At 9 °C and above the smooth lines are the best fits to a single exponential. At 4 °C, the smooth line is the best fit of the data to a double exponential. (B) Time courses of ATP binding to actomyosin V and VI. Data are of individual, unaveraged transients. A total of 0.1 μM pyrene actomyosin V was mixed with 2 mM ATP. A total of 0.1 μM pyrene actomyosin VI was mixed with 20 mM ATP. The smooth line through the actomyosin V data is the best fit to a single exponential. The smooth line through the actomyosin VI data is the best fit to a double exponential. (C) [ATP] dependence of the observed rate (k_{obs}) of ATP binding to pyrene actomyosin VI at 37 (○), 30 (□), 25 (●), 19 (▲), 14 (■), 9 (▼), and 4 (◆) °C. The solid lines are the best fits to a rectangular hyperbola (eq 12). The maximum rates of ATP binding (k_{+2T}) and the collision complex affinity ($1/K_{1T}$) used in the fits are reported in Table 1.

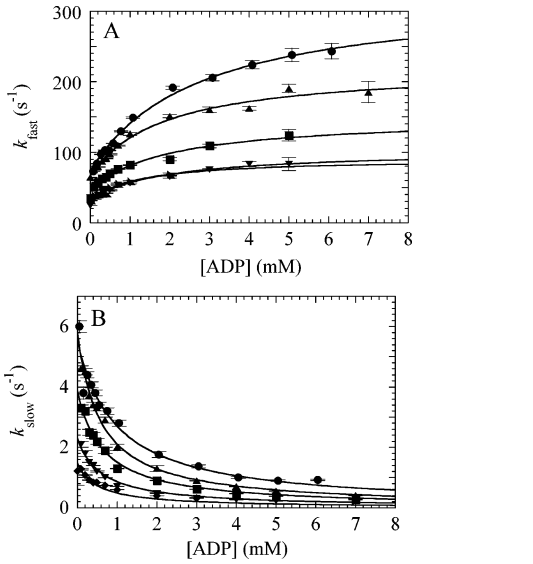

FIGURE 3: Temperature dependence of ADP binding to actomyosin VI measured by kinetic competition. (A) [ADP] dependence of the fast relaxation rate constant at 25 (●), 19 (▲), 14 (■), 9 (▼), and 4 (◆) °C in the presence of 5 mM ATP (25−9 °C) or 8 mM ATP (4 °C). The solid lines are the best fits to eq 14. The maximum rates of ADP binding (k_{+2D}) and the collision complex affinity ($1/K_{1D}$) obtained from the fits are reported in Table 1. (B) [ADP] dependence of the slow phase observed rate constant at 25 (●), 19 (▲), 14 (■), 9 (▼), and 4 (◆) °C in the presence of 5 mM ATP (25−9 °C) or 8 mM ATP (4 °C). The solid lines are the best fits to eq 15 with intercept values reported in Table 1 as k_{-2D} (ADP release).

2B). Therefore, the lag phase is specific for actomyosin VI and does not result from mixing or instrumentation artifacts. To fit the lag phase, the single exponential rise (with the observed rate constant that depends hyperbolically on [ATP]) is supplemented by a very fast exponential decay (>100 s^{-1}) that has a positive amplitude (A_i in eq 1).

In the presence of Ca^{2+} (100 μM free) and calmodulin (10 μM), the time courses of 20 mM ATP binding were essentially identical (data not shown), indicating that neither the mechanism nor the rate constants governing nucleotide binding are affected by calcium at saturating [ATP].

Lag phases arise when two sequential steps leading to formation of the product (i.e., species generating the signal being measured) have comparable rate constants (i.e., differ by less than an order of magnitude). The lag phase in ATP binding to actomyosin VI at 4 °C means that the fast exponential decay predicted by Scheme 1 (the first term in eq 13) is comparable to k_{+2T} and slow enough to be experimentally observed (i.e., <1000 s^{-1}). This also indicates that the sum of the association and dissociation rate constants ($k_{+1T}[ATP] + k_{-1T}$) for formation of the actomyosin VI−ATP collision complex [AM(ATP) in Scheme 2] is much slower than for the formation of the actomyosin V−ATP collision complex, which is completed in the dead time of the instrument.

At temperatures >25 °C, the association constant for the collision complex [AM(ATP)] formation is extremely weak ($K_{1T} \gg 12$ mM) and ATP binding cannot be saturated over the ATP concentration range examined. Thus, a reliable estimate of K_{1T} and k_{+2T} cannot be obtained. However, it is clear from the data acquired over the [ATP] range examined that the maximum observed rate constant (k_{+2T}) is >400 s^{-1} at >25 °C and can reach >600 s^{-1} at physiological temperature. Note however, that the overall ATP binding is still very slow (~100 s^{-1}) at physiological [ATP] (~2 mM) and temperature.

E. Mechanism and Temperature Dependence of ADP Binding to Actomyosin VI. As with actomyosin V, ADP binding to actomyosin VI was investigated using a kinetic competition approach. Time courses of actomyosin VI binding to a mixture of ADP and ATP are biphasic (*10*) over the 9−25 °C temperature range (data not shown), with fast and slow phases that depend on the [ADP] (Figure 3). At 4 °C, time courses of actomyosin VI binding to a mixture of ADP and ATP (Figure 4) display a lag phase in addition to the biphasic feature defined by fast and slow observed rate constants that depend on [ADP]. The lag phase arises from the slow formation (comparable to k_{+2T} in the two-step

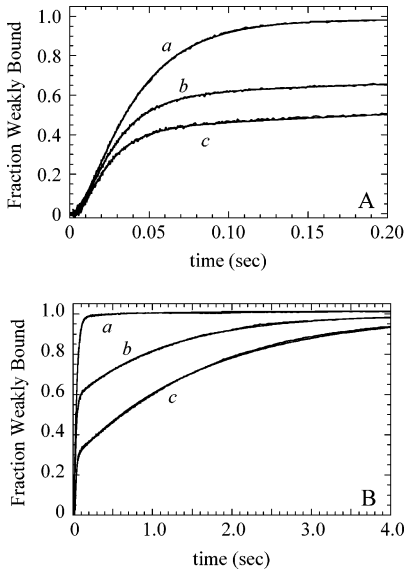

FIGURE 4: Time courses of ADP binding to actomyosin VI at 4 °C measured by kinetic competition with ATP. (A and B) Time courses of fluorescence enhancement when 0.2 μM pyrene actomyosin VI is mixed with 8 mM ATP supplemented with 30 μM ADP (curve a), 0.5 mM ADP (curve b), or 1 mM ADP (curve c). Data are of individual, unaveraged transients. The smooth lines through the data represent the best fits to a triple exponential.

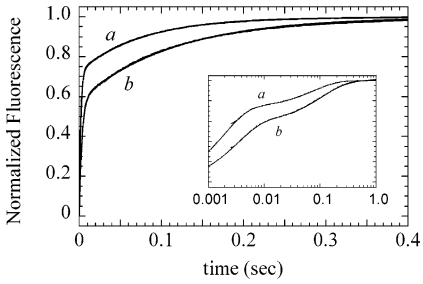

FIGURE 5: ADP dissociation from actomyosin V and VI−ADP at 25 °C. (Curve a) Actomyosin V (0.25 μM) was pre-equilibrated with 1 μM ADP and rapidly mixed with 2 mM ATP. The biphasic time course was fit to a double exponential with a slow phase (13.0 s^{-1}) corresponding to ADP release (Table 1). (Curve b) Actomyosin VI (0.25 μM) was pre-equilibrated with 30 μM ADP and rapidly mixed with 20 mM ATP. The biphasic time course was fit to a double exponential with a slow phase (6.9 s^{-1}) corresponding to ADP release (Table 1). (Inset) Same data with the *x* axis plotted on a logarithmic scale.

reaction depicted in Scheme 1) of the actomyosin−ATP collision complex at low temperatures. The time courses are well-fitted by triple exponentials, where one fast phase (completed in a few milliseconds) with a positive amplitude accounts for the observed lag phase. The fast phase was analyzed (eq 14) to obtain the rate and equilibrium constants for two-step ADP binding (K_{1D} and k_{+2D} in Scheme 2 and Table 1). The slow phase (fit to eq 15) yielded the ADP dissociation rate constants (k_{-2D}, Table 1).

F. Kinetics of ADP Release from Pre-equilibrated Actomyosin V−ADP and VI−ADP. The rates of ADP release (k_{-2D}) were confirmed by equilibrating pyrene−actomyosin with ADP (concentrations comparable to the equilibrium dissociation constant, K_d, for ADP binding: 1 μM for actomyosin V and 30 μM for actomyosin VI) and competing off with saturating ATP (2 mM for actomyosin V and 20 mM for actomyosin VI). The observed time courses are biphasic, with the fast phase reflecting ATP binding to free actomyosin and the slow phase reporting ADP release and subsequent ATP binding (Figure 5 and Table 1). The ADP release rate constants are comparable to those obtained from the slow phases of the kinetic competition assays (Figure 1D and 3B) at all temperatures examined (Table 1).

Kinetic simulations using Scheme 2 and the rate and equilibrium constants reported in Table 1 accurately reproduced the actomyosin V and VI kinetic competition experimental data (data not shown).

G. Thermodynamics of Nucleotide Binding to Actomyosin V and VI. The energetics of nucleotide binding to actomyosin V and VI were determined from the temperature dependence of the equilibrium constants.

van't Hoff plots of actomyosin V−ATP and actomyosin VI−ATP collision complex formation (K_{1T}, Figure 6A) are linear. The actomyosin V−ATP collision complex affinity (K_{1T}) consists of a large, favorable (exothermic) enthalpy change ($-\Delta H°$), which overcomes an unfavorable entropy change ($-\Delta S°$, Table 2). The contributions to actomyosin VI collision complex affinity are opposite to those of actomyosin V, with unfavorable enthalpy ($+\Delta H°$) and large, favorable entropy changes ($+\Delta S°$, Table 2).

van't Hoff plots for actomyosin−ADP collision complex formation (K_{1D}) are linear for both actomyosin V and VI and indicate that large, favorable enthalpy changes ($-\Delta H°$) overcome unfavorable entropy changes ($-\Delta S°$) associated with an initial encounter (Figure 6B and Table 3).

Strong ADP binding (K_{2D}) displays a nonlinear van't Hoff relation and occurs with a significant positive change in the molar heat capacities of both actomyosins V and VI (Figure 6C and Table 3). At >15 °C, the actomyosin V−ADP and actomyosin VI−ADP isomerization occurs with favorable entropy changes ($+\Delta S°$) and unfavorable enthalpy changes ($+\Delta H°$; Table 3), and at <15 °C, the isomerization has favorable enthalpy ($-\Delta H°$).

H. Effect of Sucrose on Nucleotide Binding to Actomyosin V and VI at 25 °C. We investigated the viscosity and osmotic pressure dependence of nucleotide binding using sucrose (Figure 7) because it does not bind to most protein surfaces (*30*, *31*).

Sucrose slows the rates of ADP isomerization (k_{+2D}) and ADP release (k_{-2D}) for both actomyosin V and VI (data not shown). At 45% (w/v) sucrose (η = 7.7 cP), ADP release (k_{-2D}) from actomyosin V is reduced ~3-fold, and the rate of ADP isomerization (k_{+2D}) is slowed ~3-fold as well; therefore, sucrose has no net effect on the equilibrium constant for strong ADP binding (K_{2D}; Figure 7C) and the corresponding free energy change for this transition. Sucrose had smaller but also proportional effects on the maximum rates of ADP binding (k_{+2D}) and dissociation (k_{-2D}) from actomyosin VI (data not shown). Therefore, sucrose dampens ADP-dependent kinetic transitions of actomyosin V and VI but not the overall equilibrium constant for strong ADP binding.

Interpreting the effects of sucrose on the equilibrium constants governing ADP binding (parts B and C of Figure 7) according to established principles of water activity [eq 7 (*24*, *32*)] indicates that ADP binding to actomyosin V and VI occurs with minimal changes in hydration (Table 3).

Sucrose has minimal effects on the actomyosin V−ATP collision complex but surprisingly weakens the formation

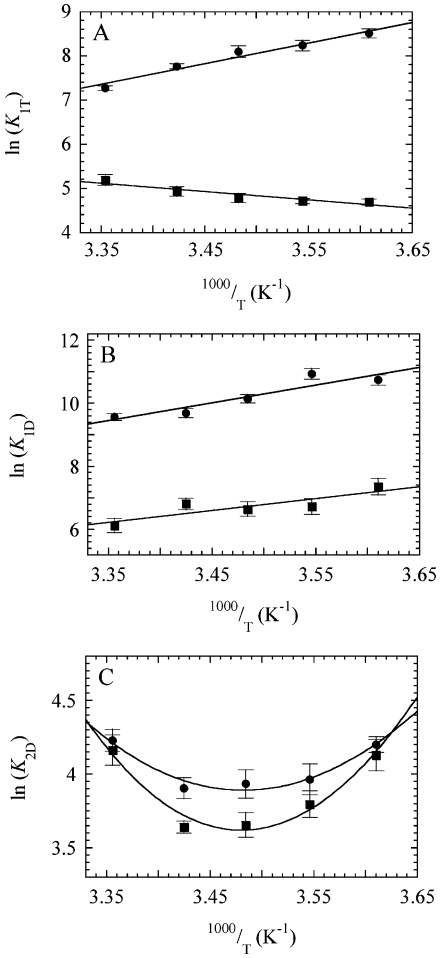

FIGURE 6: Temperature dependence of equilibrium constants for ATP and ADP binding to actomyosin V and VI. (A) van't Hoff plot of the collision complex equilibrium constant (K_{1T}) for ATP binding to actomyosin V (●) and VI (■). Thermodynamic parameters are reported in Table 2. (B) van't Hoff plot of the collision complex equilibrium constant (K_{1D}) for ADP binding to actomyosin V (●) and VI (■). (C) van't Hoff plot of the isomerization equilibrium constant (K_{2D}) for strong ADP binding to actomyosin V (●) and VI (■). Note the different ordinate scales for the different panels. Linear van't Hoff plots were fitted to the eq 3. Nonlinear van't Hoff plots were fitted to eq 5 where $\Delta C_P°$, $\Delta H°$, and $\Delta S°$ were allowed to vary in the fitting procedure. Thermodynamic parameters are reported in Tables 2 and 3.

Table 2: Thermodynamics of ATP Binding to Actomyosin V and VI at 25 °C[a]

$$AM + ATP \underset{}{\overset{K_{1T}}{\rightleftharpoons}} AM(ATP) \underset{k_{-2T}}{\overset{k_{+2T}}{\rightleftharpoons}} AM.ATP$$

parameter	myosin V−S1	myosin VI−S1
collision complex formation (K_{1T})		
$\Delta G°$ (kcal mol^{-1})[b]	−4.4 (±0.1)	−3.0 (±0.1)
$\Delta H°$ (kcal mol^{-1})[c]	−9.3 (±1.0)	3.8 (±0.8)
$\Delta S°$ (cal mol^{-1} K^{-1})[d]	−16.8 (±1.9)	22.9 (±4.9)
$-T\Delta S°$ (kcal mol^{-1})	5.0 (±0.7)	−6.8 (±1.4)
n (change in hydration)[e]	2 (±1)	18 (±1)

[a] Conditions: 50 mM KCl, 2 mM $MgCl_2$, 1 mM EGTA, 1 mM DTT, and 10 mM imidazole at pH 7.0 and 25 °C. [b] Calculated from eq 2. [c] Calculated from eq 3. [d] Calculated from eq 4. [e] Change in the number of bound water molecules.

of the actomyosin VI−ATP collision complex (Figure 7A), consistent with an increase in hydration [Table 2 (*24*, *32*, *33*)] being coupled to collision complex formation and/or a less compact (i.e., expanded) conformation (*34*, *35*) of the actomyosin VI−ATP collision complex.

Table 3: Thermodynamics of ADP Binding to Actomyosin V and VI at 25 °C[a]

$$AM + ADP \underset{}{\overset{K_{1D}}{\rightleftharpoons}} AM(ADP) \underset{k_{-2D}}{\overset{k_{+2D}}{\rightleftharpoons}} AM.ADP$$

parameter	myosin V−S1	myosin VI−S1
collision complex formation (K_{1D})		
$\Delta G°$ (kcal mol^{-1})[b]	−5.7 (±0.1)	−3.7 (±0.1)
$\Delta H°$ (kcal mol^{-1})[c]	−11.1 (±2.7)	−7.5 (±2.5)
$\Delta S°$ (cal mol^{-1} K^{-1})[d]	−18.1 (±2.5)	−12.8 (±4.3)
$-T\Delta S°$ (kcal mol^{-1})	5.4 (±0.7)	3.8 (±1.2)
n (change in hydration)[e]	7 (±4)	−1 (±1)
isomerization equilibrium ($K_{2D} = k_{+2D}/k_{-2D}$)		
$\Delta G°$ (kcal mol^{-1})[b]	−2.5 (±0.1)	−2.4 (±0.1)
$\Delta H°$ (kcal mol^{-1})[f]	10.2 (±1.7)	16.6 (±2.5)
$\Delta S°$ (cal mol^{-1} K^{-1})[f]	42.7 (±5.9)	63.8 (±8.5)
$-T\Delta S°$ (kcal mol^{-1})	−12.7 (±1.8)	−19.0 (±2.5)
$\Delta C_P°$ (kcal mol^{-1} K^{-1})[f]	0.95 (±0.17)	1.56 (±0.22)
n (change in hydration)[e]	1 (±3)	5 (±2)

[a] Conditions: 50 mM KCl, 2 mM $MgCl_2$, 1 mM EGTA, 1 mM DTT, and 10 mM imidazole at pH 7.0 and 25 °C. [b] Calculated from eq 2. [c] Calculated from eq 3. [d] Calculated from eq 4. [e] Change in the number of bound water molecules. [f] Calculated from eq 5.

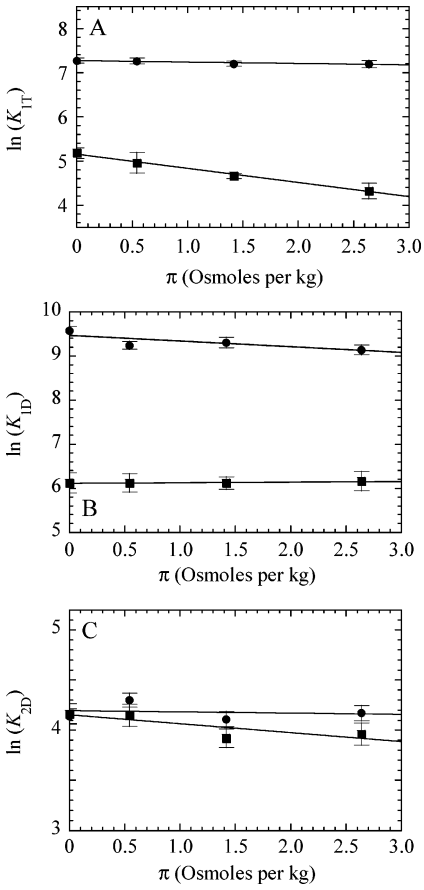

FIGURE 7: Effect of sucrose on nucleotide binding to actomyosin V and VI at 25 °C. (A) Dependence of the actomyosin V (●) and VI (■) collision complex equilibrium (K_{1T}) on osmotic pressure. (B) Dependence of the actomyosin V (●) and VI (■) collision complex equilibria (K_{1D}) on osmotic pressure. (C) Dependence of the isomerization equilibrium for strong ADP binding (K_{2D}) on osmotic pressure for actomyosin V (●) and VI (■). Solid lines represent the best fits to eq 6. The changes in hydration (n) are reported in Tables 2 and 3.

Scheme 4

$$AM_c \underset{}{\overset{K_{1Ta}}{\rightleftharpoons}} AM_o + ATP \overset{K_{1Tb}}{\rightleftharpoons} AM(ATP) \underset{k_{-2T}}{\overset{k_{+2T}}{\rightleftharpoons}} A^*M.ATP \overset{k_{diss}}{\rightarrow} A^* + M.ATP$$

Scheme 5

$$AM + ATP \overset{K_{1Ta}}{\rightleftharpoons} AM(ATP) \underset{k_{-1Tb}}{\overset{k_{+1Tb}}{\rightleftharpoons}} AM.ATP \underset{k_{-2T}}{\overset{k_{+2T}}{\rightleftharpoons}} A^*M.ATP \overset{k_{diss}}{\rightarrow} A^* + M.ATP$$

DISCUSSION

A. Mechanism of ATP Binding to Actomyosin V and VI. ATP binding to actomyosin V and VI can be modeled as a two-step process (Scheme 1) at all temperatures examined. At 4 °C, (k_{+1T}[ATP] + k_{-1T}) and k_{+2T} of actomyosin VI are comparable, which generates a lag phase in the time courses at high [ATP] (Figure 2B). Because the lag phase is observed with millimolar ATP, the magnitude of k_{+1T} for actomyosin VI must be much lower than that expected for a diffusion-limited reaction [$\sim 10^9$ M^{-1} s^{-1}, calculated using the Smoluchowski relation (*22*)], indicating that AM(ATP) is not a true collision complex limited by diffusional encounter and that some element lowers the probability of productive interaction with the nucleotide-binding site.

A mechanism where actomyosin VI equilibrates between two conformations, one competent to bind ATP (open state AM_o) and one that is not (closed state AM_c), followed by rapid, two-step ATP binding (i.e., first-order isomerization followed by a two-step transition, Scheme 4) can account for the experimental data, including the slower than diffusion-limited k_{+1T} and a weak (Table 1), temperature-dependent (Figure 6A) K_{1T} that is affected by the solution osmotic pressure (Figure 7A). According to this mechanism, the experimentally observed association constant K_{1T} in Scheme 1 contains contributions from the isomerization and encounter equilibria in Scheme 4 ($K_{1T} = K_{1Ta}K_{1Tb}$), and the observed encounter rate constant k_{+1T} in Scheme 1 is given by

$$k_{+1T} = k_{+1Ta}\left(\frac{k_{+1Tb}[ATP]}{k_{-1Ta} + k_{+1Tb}[ATP]}\right) \qquad (18)$$

which reflects the closed−open isomerization rate constant (k_{+1Ta}) times the probability [k_{+1Tb}[ATP]/(k_{-1Ta} + k_{+1Tb}[ATP])] that the open state will bind ATP rather than isomerize back to the closed state. At saturating ATP, k_{+1Tb}[ATP] ≫ k_{-1Ta}; therefore, k_{-1Ta} can be ignored, and eq 18 simplifies to k_{+1Ta}, the closed−open isomerization rate constant.

At all temperatures examined, ATP binding to actomyosin VI is very slow and K_{1T} is very weak, suggesting that the isomerization equilibrium favors the closed state (K_{1Ta} = $k_{+1Ta}/k_{-1Ta} \ll 1$ and $k_{-1Ta} \gg k_{+1Ta}$). If the equilibrium favored AM_o, the second-order association rate constant of ATP would be typical for the binding of a small molecule to a macromolecule (1−10 μM^{-1} s^{-1}).

To account for the lag phase at low temperatures, two relaxations in Scheme 4 must be comparable at temperatures <9 °C. If we assume that K_{1Tb} is a diffusion-limited rapid equilibrium as observed with other myosins, then the closed−open isomerization rate constant must be comparable to the observed maximum ATP-binding rate constant ($k_{+1Ta} \sim k_{+2T}$ at saturating [ATP]) to generate a lag phase in the time courses of ATP binding. Presumably, the lag is not observed at high temperatures (>9 °C) because the isomerization rate constant is more rapid than k_{+2}.

Multiple nucleotide-free actomyosin conformations with distinct ATP-binding properties have been observed for some myosin I isoforms (*36*). In this particular case, the isomerization equilibrium at 20 °C is near unity and the interconversion is slow (~ 8 s^{-1}) compared to ATP binding (*36*); therefore, time courses follow double exponentials with a fast phase corresponding to ATP binding to AM_o and a slow phase limited by the AM_c−AM_o isomerization. Actomyosin VI differs from actomyosin Ic in that the open−closed equilibrium strongly favors the closed state and the isomerization rate constant is rapid.

The load could affect the open−closed equilibrium and rate constants (*37*) and therefore potentially serve to favor either conformation depending on the direction of the applied stress. The slow and weak ATP binding to actomyosin VI could be attributed to a unique amino acid insert (residues ~280−300) in the head domain, whose conformation is hypothesized (*10*) to be mediated by an external (*11*) and intramolecular (*10*) load and/or unfavorable conformations of the P-loop or Loop 1. The fact that the kinetics of ATP and ADP binding are affected differently by load (*11*) suggests that the transition that weakens ATP binding to actomyosin VI may be distinct for ADP. The lower affinity of the ATP collision complex suggests that ATP binding to actomyosin VI requires greater conformational rearrangement than ADP binding, consistent with an observable sensitivity to osmotic stress (Figure 7A).

Myosin V in the absence of actin adopts a structural state that cannot accommodate bound ATP (*38*) without reorganization of the nucleotide-binding elements and switches. ATP binding to actomyosin V may therefore also follow a mechanism defined by Scheme 4. The temperature dependence of K_{1T} (Figure 6A) is consistent with such a mechanism. However, the isomerization between open and closed states must be very rapid for actomyosin V because it can be treated as a rapid equilibrium even at saturating ATP, suggesting that the extent of conformational rearrangement required to accommodate bound ATP is much smaller for actomyosin V than for actomyosin VI. The ~10-fold tighter actomyosin V−ATP collision complex affinity suggests that larger changes of the nucleotide binding switches and elements are required to accommodate bound ATP.

A mechanism where ATP binds with a collision complex followed by two sequential isomerizations of approximately equal rate prior to rapid actin dissociation (Scheme 5; pyrene fluorescence enhancement occurs with the formation of A*M·ATP) can also account for the data. However, we favor Scheme 5 for the reasons stated above.

B. Thermodynamics of Nucleotide Binding. Formation of the ATP collision complexes is surprisingly temperature-dependent for both actomyosin V and VI, suggesting they are not true collision complexes but require significant conformational rearrangement to form, consistent with the reaction scheme depicted in Scheme 4.

Formation of the ADP collision complex at 25 °C occurs with negative changes in enthalpy and entropy for both actomyosin V and VI. The enthalpic and entropic contributions to the free energy of actomyosin V−ATP and actomyosin V−ADP collision complex formation are compa-

rable. However, the energetic contributions to the actomyosin VI−ATP collision complex are opposite depending on the nucleotide ($+\Delta H°$ and $+\Delta S°$ for ATP but $-\Delta H°$ and $-\Delta S°$ with ADP), suggesting that fundamentally different mechanisms govern the recognition and specificity of ATP and ADP binding by actomyosin VI.

The equilibrium constant defining the isomerization that leads to strong ADP binding (K_{2D}) is and coupled to a large positive $\Delta C_P°$ (Table 3) for both actomyosin V and VI. This means that $\Delta H°$ for ADP binding depends on the temperature. At >15 °C, strong ADP binding to actomyosin V and VI occurs with positive $\Delta H°$. However a large positive $\Delta S°$ overcomes the unfavorable enthalpy changes and favors strong ADP binding.

Actomyosin V binds ADP ~30-fold more tightly than does actomyosin VI ($1/K_{1D}K_{2D} = 1.1$ μM for actomyosin V versus 34 μM for actomyosin VI). At 25 °C, the strong ADP-binding equilibria (K_{2D}) are comparable for actomyosin V and VI, and the different overall ADP affinities arise from differences in the ADP collision complex affinity (K_{1D}).

Overall ADP binding to actomyosin II (*39*) occurs with favorable changes in enthalpy ($\Delta H° = -4.5$ kcal mol^{-1} at 12 °C) and entropy ($\Delta S° = +3.5$ cal mol^{-1} K^{-1} at 12 °C) and little or no change in the heat capacity ($\Delta C_P° \approx 0$), as expected if ADP binding increased the number of isoenergetic conformations of the actomyosin complex. Overall ADP binding to actomyosin V and VI occurs with positive $\Delta C_P°$ and $\Delta S°$ at 25 °C because of the energetics of the weak−strong ADP-binding isomerization (Table 3).

C. Potential Sources and Molecular Origins of the Observed Positive $\Delta C_P°$ Accompanying Strong ADP Binding to Actomyosin V and VI. Changes in $\Delta C_P°$ that occur with ligand binding are typically dominated by changes in the solvent (surface effects from polar and nonpolar residues), changes in vibrational modes of the protein−ligand complex, and/or obligatory coupling of temperature-dependent equilibria (*40*, *41*).

Most characterized protein−ligand association reactions that display a change in heat capacity occur with negative $\Delta C_P°$ values, which are often attributed to water reorganization arising from a reduction in the accessible hydrophobic surface areas accompanying complex formation (i.e., the hydrophobic effect). Positive $\Delta C_P°$ values are less common and are typically attributed to an increased solvent-exposed hydrophobic surface area (*42*, *43*), dehydration of polar surface areas (*44*), or structural transitions in the bimolecular complex (*45*, *46*).

If the positive $\Delta C_P°$ accompanying strong ADP binding arose from the hydrophobic effect (i.e., solvent exposure of hydrophobic surface or dehydration/burial of polar surface area), its magnitude, which is on the scale on some protein unfolding reactions, would implicate a rather large change in the total accessible surface area (ΔASA_{tot}) of actomyosin [~6200 Å^2 for actomyosin V and ~10 600 Å^2 for actomyosin VI; calculated using the empirical relation, which does not distinguish between contributions from polar and hydrophobic areas: ΔASA_{tot} (in Å^2) = $\Delta C_P°$ (in cal mol^{-1} K^{-1})/0.147 (*47*)]. Such large changes in accessible surface area are hard to reconcile with the molecular dimensions of myosin VI (*4*) and helical reconstruction of myosin VI-decorated actin filaments (*48*). In addition, the fact that binding of few water molecules is coupled to the ADP intramolecular isomerization (K_{2D}) of actomyosin V [1 (±3), Figure 7 and Table 3] and VI [5 (±2), Figure 7 and Table 3] strongly suggests that solvent reordering does not generate the positive $\Delta C_P°$.

There is a considerable body of evidence indicating that ionic interactions and formation of ion pairs (e.g., charge neutralization of ADP) can also contribute to positive $\Delta C_P°$, $\Delta S°$, and $\Delta H°$ because of the desolvation of charged surfaces and ions (*43*, *49*, *50*). However, our osmotic stress measurements (Figure 7C) indicate that strong ADP binding (K_{2D}) is not coupled to dehydration. We, therefore, conclude that formation of ion pairs does not fully account for the observed $\Delta C_P°$.

Nonlinear van't Hoff plots and "apparent" heat capacity changes ($\Delta C_{P,app}°$) can also arise from the coupling of two (or more) equilibria with enthalpy changes ($\Delta H°$) of opposite signs even if the intrinsic heat capacity changes are negligible [$\Delta C_P° \approx 0$ (*40*, *41*)]. One potential source of a coupled equilibrium reaction is the dissociation of actomyosin with ADP binding, which weakens the actin-binding affinity of both myosin V (*13*) and VI (*5*). However, these reactions are slow and do not occur during the time course of the reaction using the kinetic competition assay. We can therefore eliminate a coupled dissociation from actin as a source of the observed nonlinear van't Hoff plots.

Additional equilibria involving structural changes of protein−ligand complexes can generate a positive $\Delta C_P°$ (*51*). Therefore, an isomerization between multiple strongly bound actomyosin−ADP states (*25*, *29*) could contribute to the observed positive $\Delta C_P°$.

The positive $\Delta C_P°$ that accompanies strong ADP binding to actomyosin V and VI and the positive $\Delta S°$ and $\Delta H°$ at 25 °C are also consistent with significant conformational rearrangement, such as an increase in the number and/or amplitudes of soft internal modes (*43*, *52*). We interpret the positive $\Delta C_P°$ and $\Delta S°$ observed with strong ADP binding to actomyosin V and VI to reflect an increased disorder of the strongly bound actomyosin−ADP complex. The disorder could arise from fluctuations *within* an energy state and/or *among* different ones (i.e., between states of different energies and/or low frequency, vibrational modes of an individual energy state). ADP binding to actomyosin may lower the energy difference between two (or more) otherwise inaccessible conformational states (*53*), which would generate positive $\Delta C_P°$ and $\Delta S°$ because of the population distribution among the multiple states. Such a process would be expected to increase the elasticity and lower the stiffness of the actomyosin complex. While we favor an interpretation where the conformational sampling arises from the myosin, changes in actin filament dynamics (*54*) could potentially contribute to the observed positive $\Delta C_P°$ and $\Delta S°$. The greater $\Delta C_P°$ and $\Delta S°$ of actomyosin VI (Table 3) may reflect greater ADP-induced flexibility than for actomyosin V.

The increased elasticity may propagate to regions outside of the nucleotide-binding site and possibly the proximal tail region of myosin VI. If the conformation of the myosin VI proximal tail (*55*), which is absent from the myosin VI construct used in this study, is nucleotide-dependent, the source of the allostery must originate at the nucleotide-binding site.

D. Implications for Actomyosin Force Generation. ADP binding to some myosins (those with ADP affinities ≤ 10 μM) including actomyosin VI (*48*) induces a rotation of the

lever arm relative to the motor domain (*37*). Single-molecule studies demonstrate that ADP release from these actomyosin classes generates a mechanical displacement and contributes to the overall working stroke (*4*, *56*). We suggest that sucrose reduces the rate constants of both ADP binding and release by suppressing the lever arm rotation that accompanies strong ADP binding to actomyosin V and VI (*37*, *48*, *57*). The effect is not due to changes in the chemical potential of the reactants because sucrose does not change the equilibrium constant of this transition (Figure 7C). Sucrose must therefore dampen some kinetic process. Solvent microviscosity restricts the structural dynamics and conformational flexibility of proteins (*58*−*60*) and would therefore inhibit both association and dissociation if the weak−strong ADP-binding transition is coupled to rotation of the regulatory domain lever arm. Increased rotational flexibility of the lever arm upon ADP isomerization would be expected to generate positive entropy and heat capacity changes as observed (Table 3).

The weak−strong actin-binding transition associated with force generation and P_i release is accompanied by a disorder−order transition in muscle myosin (for a review, see ref *61*). Multiple lever arm orientations exist prior to P_i release (*62*), and P_i release merely shifts the distribution between these two lever arm orientations toward the "post power stroke" orientation, resulting in a net displacement and force generation.

We hypothesize that the energetics governing strong ADP binding and release reflect, on a smaller scale, those that occur with P_i release and the power stroke. The actomyosin ATPase cycle can therefore be viewed as an energetic landscape where sequential product release (P_i and ADP) progressively increases the order of actomyosin and favors the population of a "post power stroke" lever arm position.

ACKNOWLEDGMENT

We thank anonymous reviewers for critical evaluation of the manuscript.

REFERENCES

1. Berg, J. S., Powell, B. C., and Cheney, R. E. (2001) A millennial myosin census, *Mol. Biol. Cell 12*, 780−794.
2. Geeves, M. A., and Holmes, K. C. (1999) Structural mechanism of muscle contraction, *Annu. Rev. Biochem. 68*, 687−728.
3. De La Cruz, E. M., and Ostap, E. M. (2004) Relating biochemistry and function in the myosin superfamily, *Curr. Opin. Cell Biol. 16*, 61−67.
4. Lister, I., Schmitz, S., Walker, M., Trinick, J., Buss, F., Veigel, C., and Kendrick-Jones, J. (2004) A monomeric myosin VI with a large working stroke, *EMBO J. 23*, 1729−1738.
5. De La Cruz, E. M., Ostap, E. M., and Sweeney, H. L. (2001) Kinetic mechanism and regulation of myosin VI, *J. Biol. Chem. 276*, 32373−32381.
6. Rock, R. S., Rice, S. E., Wells, A. L., Purcell, T. J., Spudich, J. A., and Sweeney, H. L. (2001) Myosin VI is a processive motor with a large step size, *Proc. Natl. Acad. Sci. U.S.A. 98*, 13655−13659.
7. Nishikawa, S., Homma, K., Komori, Y., Iwaki, M., Wazawa, T., Hikikoshi Iwane, A., Saito, J., Ikebe, R., Katayama, E., Yanagida, T., and Ikebe, M. (2002) Class VI myosin moves processively along actin filaments backward with large steps, *Biochem. Biophys. Res. Commun. 290*, 311−317.
8. Sakamoto, T., Amitani, I., Yokota, E., and Ando, T. (2000) Direct observation of processive movement by individual myosin V molecules, *Biochem. Biophys. Res. Commun. 272*, 586−590.
9. Veigel, C., Wang, F., Bartoo, M. L., Sellers, J. R., and Molloy, J. E. (2002) The gated gait of the processive molecular motor, myosin V, *Nat. Cell Biol. 4*, 59−65.
10. Robblee, J. P., Olivares, A. O., and de la Cruz, E. M. (2004) Mechanism of nucleotide binding to actomyosin VI: Evidence for allosteric head−head communication, *J. Biol. Chem. 279*, 38608−38617.
11. Altman, D., Sweeney, H. L., and Spudich, J. A. (2004) The mechanism of myosin VI translocation and its load-induced anchoring, *Cell 116*, 737−749.
12. Rosenfeld, S. S., and Sweeney, H. L. (2004) A model of myosin V processivity, *J. Biol. Chem. 279*, 40100−40111.
13. De La Cruz, E. M., Wells, A. L., Rosenfeld, S. S., Ostap, E. M., and Sweeney, H. L. (1999) The kinetic mechanism of myosin V, *Proc. Natl. Acad. Sci. U.S.A. 96*, 13726−13731.
14. De La Cruz, E. M., Sweeney, H. L., and Ostap, E. M. (2000) ADP inhibition of myosin V ATPase activity, *Biophys. J. 79*, 1524−1529.
15. De La Cruz, E. M., Wells, A. L., Sweeney, H. L., and Ostap, E. M. (2000) Actin and light chain isoform dependence of myosin V kinetics, *Biochemistry 39*, 14196−14202.
16. Brizzard, B. L., Chubet, R. G., and Vizard, D. L. (1994) Immunoaffinity purification of FLAG epitope-tagged bacterial alkaline phosphatase using a novel monoclonal antibody and peptide elution, *BioTechniques 16*, 730−735.
17. Pardee, J. D., and Spudich, J. A. (1982) Purification of muscle actin, *Methods Enzymol. 85* (part B), 164−181.
18. Kouyama, T., and Mihashi, K. (1981) Fluorimetry study of *N*-(1-pyrenyl)iodoacetamide-labelled F-actin. Local structural change of actin protomer both on polymerization and on binding of heavy meromyosin, *Eur. J. Biochem. 114*, 33−38.
19. Johnson, K. A., Shimizu, T., and Holzbaur, E. L. (1983) Kinetic evidence for multiple dynein heads: Modeling the dissociation reaction, *J. Biol. Chem. 258*, 13847−13848.
20. Shimizu, T., and Johnson, K. A. (1983) Kinetic evidence for multiple dynein ATPase sites, *J. Biol. Chem. 258*, 13841−13846.
21. Barshop, B. A., Wrenn, R. F., and Frieden, C. (1983) Analysis of numerical methods for computer simulation of kinetic processes: Development of KINSIM−A flexible, portable system, *Anal. Biochem. 130*, 134−145.
22. Talavera, M. A., and De La Cruz, E. M. (2005) Equilibrium and kinetic analysis of nucleotide binding to the DEAD-box RNA helicase DbpA, *Biochemistry 44*, 959−970.
23. Wolf, A. V., Brown, M. G., and Prentiss, P. C. (1986) *CRC Handbook of Chemistry and Physics*, CRC Press, Boca Raton, FL.
24. Parsegian, V. A., Rand, R. P., and Rau, D. C. (1995) Macromolecules and water: Probing with osmotic stress, *Methods Enzymol. 259*, 43−94.
25. Hannemann, D. E., Cao, W., Robblee, J. P., Olivares, A. O., and De La Cruz, E. M. (2005) Magnesium, ADP, and actin binding linkage of myosin V: Evidence for multiple myosin V−ADP and actomyosin V−ADP states, *Biochemistry*, in press.
26. Trybus, K. M., Krementsova, E., and Freyzon, Y. (1999) Kinetic characterization of a monomeric unconventional myosin V construct, *J. Biol. Chem. 274*, 27448−27456.
27. Wang, F., Thirumurugan, K., Stafford, W. F., Hammer, J. A., III, Knight, P. J., and Sellers, J. R. (2004) Regulated conformation of myosin V, *J. Biol. Chem. 279*, 2333−2336.
28. Wang, F., Chen, L., Arcucci, O., Harvey, E. V., Bowers, B., Xu, Y., Hammer, J. A., III, and Sellers, J. R. (2000) Effect of ADP and ionic strength on the kinetic and motile properties of recombinant mouse myosin V, *J. Biol. Chem. 275*, 4329−4335.
29. Rosenfeld, S. S., Houdusse, A., and Sweeney, H. L. (2004) Magnesium regulates ADP dissociation from myosin V, *J. Biol. Chem.*
30. Wang, A., Robertson, A. D., and Bolen, D. W. (1995) Effects of a naturally occurring compatible osmolyte on the internal dynamics of ribonuclease A, *Biochemistry 34*, 15096−15104.
31. Lee, J. C., and Timasheff, S. N. (1981) The stabilization of proteins by sucrose, *J. Biol. Chem. 256*, 7193−7201.
32. Rand, R. P., Fuller, N. L., Butko, P., Francis, G., and Nicholls, P. (1993) Measured change in protein solvation with substrate binding and turnover, *Biochemistry 32*, 5925−5929.
33. Highsmith, S., Duignan, K., Cooke, R., and Cohen, J. (1996) Osmotic pressure probe of actin−myosin hydration changes during ATP hydrolysis, *Biophys. J. 70*, 2830−2837.
34. Lonhienne, T. G., Jackson, C. M., and Winzor, D. J. (2003) Thermodynamic non-ideality as an alternative source of the effect of sucrose on the thrombin-catalyzed hydrolysis of peptide *p*-nitroanilide substrates, *Biophys. Chem. 103*, 259−269.

35. Minton, A. P. (2004) Models for excluded volume interaction between an unfolded protein and rigid macromolecular cosolutes: Macromolecular crowding and protein stability revisited, *Biophys. J.*
36. Geeves, M. A., Perreault-Micale, C., and Coluccio, L. M. (2000) Kinetic analyses of a truncated mammalian myosin I suggest a novel isomerization event preceding nucleotide binding, *J. Biol. Chem. 275*, 21624−21630.
37. Batters, C., Arthur, C. P., Lin, A., Porter, J., Geeves, M. A., Milligan, R. A., Molloy, J. E., and Coluccio, L. M. (2004) Myo1c is designed for the adaptation response in the inner ear, *EMBO J. 23*, 1433−1440.
38. Coureux, P. D., Wells, A. L., Menetrey, J., Yengo, C. M., Morris, C. A., Sweeney, H. L., and Houdusse, A. (2003) A structural state of the myosin V motor without bound nucleotide, *Nature 425*, 419−423.
39. Smith, S. J., White, H. D., and Woledge, R. C. (1984) Microcalorimetric measurement of the enthalpy of binding of rabbit skeletal myosin subfragment 1 and heavy meromyosin to F-actin, *J. Biol. Chem. 259*, 10303−10308.
40. Fisher, H. F., Colen, A. H., and Medary, R. T. (1981) Temperature-dependent δ C0p generated by a shift in equilibrium between macrostates of an enzyme, *Nature 292*, 271−272.
41. Ferrari, M. E., and Lohman, T. M. (1994) Apparent heat capacity change accompanying a nonspecific protein−DNA interaction. *Escherichia coli* SSB tetramer binding to oligodeoxyadenylates, *Biochemistry 33*, 12896−12910.
42. Spolar, R. S., and Record, M. T., Jr. (1994) Coupling of local folding to site-specific binding of proteins to DNA, *Science 263*, 777−784.
43. Sturtevant, J. M. (1977) Heat capacity and entropy changes in processes involving proteins, *Proc. Natl. Acad. Sci. U.S.A. 74*, 2236−2240.
44. Dragan, A. I., Klass, J., Read, C., Churchill, M. E., Crane-Robinson, C., and Privalov, P. L. (2003) DNA binding of a non-sequence-specific HMG-D protein is entropy driven with a substantial non-electrostatic contribution, *J. Mol. Biol. 331*, 795−813.
45. Fisher, H. F., and Singh, N. (1995) Calorimetric methods for interpreting protein−ligand interactions, *Methods Enzymol. 259*, 194−221.
46. Cooper, A., Johnson, C. M., Lakey, J. H., and Nollmann, M. (2001) Heat does not come in different colours: Entropy−enthalpy compensation, free energy windows, quantum confinement, pressure perturbation calorimetry, solvation, and the multiple causes of heat capacity effects in biomolecular interactions, *Biophys. Chem. 93*, 215−230.
47. Robertson, A. D., and Murphy, K. P. (1997) Protein structure and the energetics of protein stability, *Chem. Rev. 97*, 1251−1268.
48. Wells, A. L., Lin, A. W., Chen, L. Q., Safer, D., Cain, S. M., Hasson, T., Carragher, B. O., Milligan, R. A., and Sweeney, H. L. (1999) Myosin VI is an actin-based motor that moves backwards, *Nature 401*, 505−508.
49. Ross, P. D., and Subramanian, S. (1981) Thermodynamics of protein association reactions: Forces contributing to stability, *Biochemistry 20*, 3096−3102.
50. Misra, V. K., Hecht, J. L., Yang, A. S., and Honig, B. (1998) Electrostatic contributions to the binding free energy of the λcI repressor to DNA, *Biophys. J. 75*, 2262−2273.
51. Eftink, M. R., Anusiem, A. C., and Biltonen, R. L. (1983) Enthalpy−entropy compensation and heat capacity changes for protein−ligand interactions: General thermodynamic models and data for the binding of nucleotides to ribonuclease A, *Biochemistry 22*, 3884−3896.
52. Kodama, T. (1981) Reaction heats and heat capacity changes for intermediate steps of the ATP hydrolysis catalyzed by myosin subfragment 1, *J. Biol. Chem. 256*, 2928−2933.
53. Prabhu, N. V., and Sharp, K. A. (2005) Heat capacity in proteins, *Annu. Rev. Phys. Chem. 56*, 521−548.
54. Prochniewicz, E., Walseth, T. F., and Thomas, D. D. (2004) Structural dynamics of actin during active interaction with myosin: Different effects of weakly and strongly bound myosin heads, *Biochemistry 43*, 10642−10652.
55. Rock, R. S., Ramamurthy, B., Dunn, A. R., Beccafico, S., Rami, B. R., Morris, C., Spink, B. J., Franzini-Armstrong, C., Spudich, J. A., and Sweeney, H. L. (2005) A flexible domain is essential for the large step size and processivity of myosin VI, *Mol. Cell 17*, 603−609.
56. Veigel, C., Coluccio, L. M., Jontes, J. D., Sparrow, J. C., Milligan, R. A., and Molloy, J. E. (1999) The motor protein myosin-I produces its working stroke in two steps, *Nature 398*, 530−533.
57. Whittaker, M., Wilson-Kubalek, E. M., Smith, J. E., Faust, L., Milligan, R. A., and Sweeney, H. L. (1995) A 35 Å movement of smooth muscle myosin on ADP release, *Nature 378*, 748−751.
58. Priev, A., Almagor, A., Yedgar, S., and Gavish, B. (1996) Glycerol decreases the volume and compressibility of protein interior, *Biochemistry 35*, 2061−2066.
59. Somogyi, B., Norman, J. A., Zempel, L., and Rosenberg, A. (1988) Viscosity and transient solvent accessibility of Trp-63 in the native conformation of lysozyme, *Biophys. Chem. 32*, 1−13.
60. Gavish, B., and Werber, M. M. (1979) Viscosity-dependent structural fluctuations in enzyme catalysis, *Biochemistry 18*, 1269−1275.
61. Thomas, D. D., Prochniewicz, E., and Roopnarine, O. (2002) Changes in actin and myosin structural dynamics due to their weak and strong interactions, *Results Probl. Cell Differ. 36*, 7−19.
62. Baker, J. E., Brust-Mascher, I., Ramachandran, S., LaConte, L. E., and Thomas, D. D. (1998) A large and distinct rotation of the myosin light chain domain occurs upon muscle contraction, *Proc. Natl. Acad. Sci. U.S.A. 95*, 2944−2949.

BI050232G